

# Scattering of fast hydrogen particles in gaseous media

V. I. Radchenko

*Ural State Technical University, 620002 Ekaterinburg, Russia*

(Submitted 7 April 1993; resubmitted 23 December 1993)

*Zh. Eksp. Teor. Fiz.* **105**, 834–852 (April 1994)

The processes by which the hydrogen particles  $H^+$ ,  $H^0$ ,  $H^-$  interact with gaseous targets, including electron losses but excluding changes in the charged state, have been investigated in the energy range  $E=0.1\text{--}20$  MeV. The experimental apparatus, technique, and results of measuring the cross sections  $\sigma_{01}$ ,  $\sigma_{\bar{1}0}$ ,  $\sigma_{\bar{1}1}$ , are described, together with the efficiency for neutralization of  $H^-$  ions in He, Ar, Kr, Xe,  $H_2$ ,  $O_2$ ,  $CO_2$ ,  $C_2H_2$  (for  $E=1.67$  and 5.0 MeV), and also in a target of potassium vapor ( $E=5.14$  MeV). The cross sections and characteristic scattering angles for hydrogen particles with no change in the charged state and with electron losses by the  $H^-$  ions in a target made of atomic hydrogen have been calculated in the Born approximation omitting exchange processes. The same approach has been used to find formulas for the differential scattering cross sections from a Thomas–Fermi potential and a dipole potential. The concept of the instantaneous dipole moment of an electron shell in a target atom is used to derive an approximation that permits calculations of the characteristic angles and cross sections to be carried out for the  $(\bar{1}0) + (\bar{1}1)$ ,  $(00)$ ,  $(\bar{1}\bar{1})$ ,  $(11)$  processes with targets of atomic hydrogen, alkaline metals, and alkaline–halide molecules.

## 1. INTRODUCTION

Electron loss processes involving negative ions and atoms of hydrogen, as well as processes in which these particle and protons are scattered without any change in the charge in various targets, have a fundamental theoretical significance and are important for many applied problems. These include heating and diagnostics of thermonuclear plasmas, construction of tandem accelerators, mesons factories, etc. The fundamental practical problem of experimental and theoretical investigations of these processes consists in studying the conditions under which hydrogen atoms or protons form most efficiently, such that the resulting particle beam has the smallest possible angular divergence and emittance (in most cases we are concerned with finding a compromise between these last two conditions). The problem is considered to be solved, first, by determining the differential and total cross sections for loss (capture) of electrons, the efficiency with which  $H^-$  ions are neutralized, and also the angular distributions and typical scattering angles for particles in the processes  $(\bar{1}0)$ ,  $(\bar{1}\bar{1})$ ,  $(01)$ ; in the next stage it is necessary to study the cross sections and angular properties of the  $(\bar{1}\bar{1})$ ,  $(00)$ ,  $(11)$  particle scattering processes in which there is no change in charge and  $(\bar{1}0)$  collisions in which hydrogen atoms are formed in an excited state (in particular, in the  $2s_{1/2}$ -metastable state and in long-lived and Rydberg states). The formation of  $H^0(nl)$  ions in an excited state turns out in a number of cases to exert a significant (usually negative) influence on their transport and makes the beam “visible,” something that needs to be either suppressed (say, in order to prepare the initial beam in  $H^0(1s) + M \rightarrow H^-, H^0(nl), H^+ + \dots$  experiments), or exploited (e.g., to determine the  $\sigma_{\bar{1}0}(nl)$  cross section in order to monitor a particle beam, etc.).

The aim of the present article is to study processes in which  $H^-$ ,  $H^0(1s)$ ,  $H^+$  hydrogen particles with energy  $E=0.1\text{--}20$  MeV are scattered, accompanied by loss of electrons but with no change in the charge of the gaseous medium.

A considerable number of papers have been devoted to electron loss processes. These are noted in the monograph of Massey,<sup>1</sup> several reviews,<sup>2–4</sup> and a number of individual papers, among which we note Refs. 5–11. Most experimental work has been performed with incident particles of energy  $E < 200$  keV and various targets. Experimental data are available for higher energies primarily in light inert (He, Ar) and simple molecular ( $H_2$ ,  $N_2$ ,  $O_2$ ,  $CO_2$ ) gases. There are no systematic measurements for other gases or for vapor targets (such as, e.g., alkaline metal vapors or alkaline–halide compounds).

Theoretical analysis and calculations of the electron loss cross sections due to negative ions and atoms of hydrogen have been carried out over the entire range of collision energies of practical importance for targets of H,  $H_2$ , N,  $N_2$ , O,  $O_2$  and inert gases. The calculations are most complete for  $E > 100$  keV, since here the powerful tool of the Born approximation is used in one modification or another. But again, there are no theoretical results for more complicated targets. Comparison of the theoretical and experimental cross sections  $\sigma_{\bar{1}0}$  reveals that they agree well for light targets, but the theoretical values are 2–3 times larger for Kr and Xe. In this connection it is appropriate to note the success of calculations in the semiclassical model of free collisions<sup>10</sup> for Kr, Xe targets, and Ref. 8 in which the three-particle Born approximation is used to find the differential cross section for the  $(\bar{1}0)$  process in inert gases.

Calculations of the partial cross sections for  $(11)$  and  $(00)$  processes in H and He targets were carried out in early papers on the physics of ion–atom collisions, which

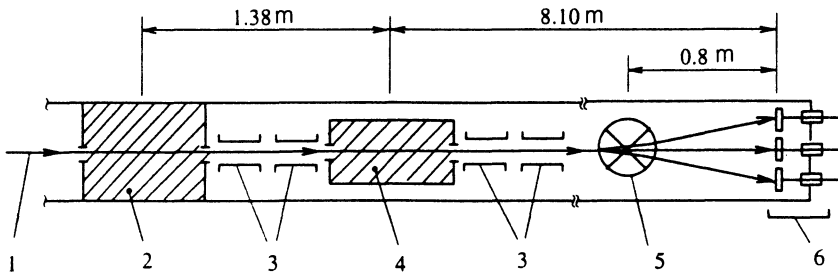


FIG. 1. View of the experimental apparatus with a vapor target: 1) collimated ion beam; 2) collision chamber; 3) electrical deflectors for controlling the beam; 4) vapor target; 5) magnet system; 6) particle detection module.

have since become classics. We therefore point out only Refs. 9 and 11–13, in which the cross sections were summed over all possible final states of the target particle, including the continuum, more complicated target atoms were used, and the  $(\bar{1}\bar{1})$  process was also studied. Only two experimental treatments are available in the high-energy region.<sup>11,14</sup> References 8, 9, and 11 are devoted to the theoretical determination of the angular behavior of  $(\bar{1}\bar{1})$ ,  $(00)$ , and  $(\bar{1}0)$  processes. D'yachkov *et al.*<sup>15</sup> measured the characteristic scattering angles for the neutralization of  $H^-$  ions.

Thus, the electron loss cross sections due to fast hydrogen particles have been studied reasonably completely only in the simplest targets. Other questions require further work. This applies most of all to the study of the angular behavior of all processes and the choice of more complicated targets.

In the present work we have measured the total cross sections for the processes  $(\bar{1}0)$ ,  $(\bar{1}\bar{1})$  and  $(01)$  when incident hydrogen particles with energies  $E=1.67$  and  $5.0$  MeV interact with He, Ar, Kr, Xe,  $H_2$ ,  $O_2$ ,  $CO_2$ ,  $C_2H_2$  gases, and at energies  $E=5.14$  MeV in potassium vapor. We have calculated cross sections and characteristic scattering angles using the Born approximation for the range  $E=0.1$ – $20$  MeV in collisions of the form  $(\bar{1}0) + (\bar{1}\bar{1})$ ,  $(\bar{1}\bar{1})$ ,  $(00)$ ,  $(11)$  involving interactions between monatomic hydrogen and Li, Na, K, Rb, Cs or NaCl, KCl, KBr, KI, CsI molecules (using the Thomas–Fermi and dipole potential models to describe the target).

In Secs. 2 and 3 we describe the technique for processing the experimental data, the apparatus, and the results of the measurements. “Exact” calculations for H targets are given in Sec. 4. In Sec. 5 we introduce expressions for the differential scattering cross sections off model interaction potentials and derive a potential which enables us to perform calculations of the cross sections for alkaline metal atoms and for alkaline–halide molecules.

## 2. DETERMINATION OF THE $\sigma_{\bar{1}0}$ , $\sigma_{\bar{1}\bar{1}}$ , $\sigma_{01}$ CROSS SECTIONS FROM MEASURED CHARGE DISTRIBUTIONS

We have processed the experimental data to determine the  $\sigma_{\bar{1}0}$ ,  $\sigma_{\bar{1}\bar{1}}$ ,  $\sigma_{01}$  cross sections in the energy range  $E \geq 0.2$  MeV, as a rule, without taking into account electron capture processes, since the capture cross sections are found to be several orders of magnitude lower than the corresponding loss cross sections.<sup>1,2</sup> The charge composition of a beam which is passed through a target of thickness  $t$  is determined by the following differential equations:

$$\frac{d\Phi_0(t)}{dt} = -\sigma_{01}\Phi_0(t) \quad (1)$$

for an initial beam of hydrogen atoms,

$$\frac{d\Phi_{\bar{1}}(t)}{dt} = -\sigma_{\Sigma}\Phi_{\bar{1}}(t), \quad (2)$$

$$\frac{d\Phi_0(t)}{dt} = \sigma_{\bar{1}0}\Phi_{\bar{1}}(t) - \sigma_{01}\Phi_0(t) \quad (3)$$

for an initial beam of  $H^-$  atoms, and the normalization condition  $\sum_i \Phi_i(t) = 1$ , where  $\Phi_i(t)$  is the fraction of beam particles with charge  $i$ , and  $\sigma_{\Sigma} = \sigma_{\bar{1}0} + \sigma_{\bar{1}\bar{1}}$ . Equations (1)–(3) respectively correspond to the three desired cross sections  $\sigma_{01}$ ,  $\sigma_{\bar{1}0}$ ,  $\sigma_{\bar{1}\bar{1}}$ . Solving them we find

$$\sigma_{01} = \frac{1}{t} \ln \frac{\Phi_0(0)}{\Phi_0(t)}, \quad (4)$$

$$\sigma_{\Sigma} = \frac{1}{t} \ln \frac{\Phi_{\bar{1}}(0)}{\Phi_{\bar{1}}(t)}, \quad (5)$$

$$\sigma_{\bar{1}0} = \frac{\sigma_{\Sigma} - \sigma_{01}}{\Phi_{\bar{1}}(0)} \frac{\Phi_0(t) - \Phi_0(0)e^{-\sigma_{01}t}}{e^{-\sigma_{01}t} - e^{-\sigma_{\Sigma}t}}, \quad (6)$$

where  $\Phi_0(0)$ ,  $\Phi_{\bar{1}}(0)$  are the initial conditions at  $t=0$ . Thus, in the first experiment the  $\Phi_i(t)$  charge distribution and  $t$  are used with Eq. (4) to find the cross section  $\sigma_{01}$ , while in the second  $\sigma_{\Sigma}$ ,  $\sigma_{\bar{1}0}$  are found successively [Eqs. (5) and (6)] and also  $\sigma_{\bar{1}\bar{1}} = \sigma_{\Sigma} - \sigma_{\bar{1}0}$ .

Using expression (6) for the efficiency  $\Phi_0^{\max}$  with which  $H^-$  ions are neutralized and the corresponding target thickness  $t^{\max}$  [taking  $\Phi_{\bar{1}}(0) = 1$ ,  $\Phi_0(0) = 0$ ] we find the following expressions:

$$\Phi_0^{\max} = \frac{\sigma_{\bar{1}0}}{\sigma_{01}} \left( \frac{\sigma_{01}}{\sigma_{\Sigma}} \right)^{\frac{\sigma_{\Sigma}}{\sigma_{\Sigma} - \sigma_{01}}}, \quad t^{\max} = \frac{1}{\sigma_{\Sigma} - \sigma_{01}} \ln \frac{\sigma_{\Sigma}}{\sigma_{01}}. \quad (7)$$

## 3. EXPERIMENTAL APPARATUS; RESULTS OF MEASUREMENTS

The essential components of the experimental apparatus and the technique used to perform the measurements are described in Refs. 11 and 16. In the present work, in studying the charged state of the beam of fast hydrogen particles, we added a module for detecting particles of different charge, a magnet system, and a vapor target for obtaining potassium vapor (Fig. 1).

The module for detecting  $H^+$ ,  $H^0$ ,  $H^-$  hydrogen particles consists of three DKPs-350 semiconductor detectors

at a distance of 28 mm from one another, positioned perpendicular to the direction in which the charged components of the beam move. The total beam intensity was measured to be  $<500$  particle/s, so the charged fractions of the beam were directed right at the detectors, which operated in a complex with standard spectrometric and counting apparatus. F5007 programmable counters in each measurement channel were connected to a single control system, which allowed the measurement of the number of incident particles to be made at the same time for all charge fractions and enabled them to end at the same time, after a prescribed number of pulses had been collected in one detection circuit (this was generally the  $H^0$  detection circuit).

After it had passed through the target the beam was broken up into charge component and the  $H^+$ ,  $H^-$  ions were directed into the central region of the detectors using the magnet system. In the design of the magnet system we used permanent magnets with dimensions  $55 \times 15$  mm<sup>2</sup> made of the alloy  $SmCo_5$ . The magnetic induction was controlled by changing the distance between the poles by means of clamps. The magnet system was located outside the ion guide; the distance between the vacuum sleeves (for transporting the beam), in which the pole positioners were shifted, was equal to 15 mm (for a ribbon beam of width 5–8 mm).

A vapor target consists of a casing, a vapor generator, and input and output slits. All these components of the vapor target were made of stainless steel, and each had its own heating system, thermal shielding, and temperature control using  $\chi A$  thermocouples. The effective length of a vapor target was 436 mm. The input and output slits with identical dimensions  $0.25 \times 5$  mm<sup>2</sup> served to limit the vapor flow. In order to prevent gas from escaping into the working volume of the vapor target its structural elements were baked at  $T=200\text{--}250$  °C for 30 h before being exposed to potassium and at  $T=100\text{--}120$  °C afterwards.

The centers of the collision chamber for admitting gas (Fig. 1) and the vapor target were separated by a distance of 1.38 m from one another, so that with the collimators used and the angular variation of the observed processes<sup>11,16</sup> the presence of the vapor target in the ion guide did not affect the results of the experiments in which the collision chamber was used. However, when more sensitive measurements were carried out in gaseous targets the separation between the collision chamber and the magnet system was minimized (in order to reduce the thickness of the residual gas target, whose composition could not be monitored) as the vapor target was moved away, and was equal to 1.2 m when the residual gas pressure was  $<3 \cdot 10^{-4}$  Pa. But the separation between the center of the vapor target and the detector unit was equal to 8.10 m (see also Ref. 16).

In the course of the measurements the initial particle charge distribution in the beam on input to the collision chamber was essentially uniform both for gases and for K vapor, and was maintained at the level  $\Phi_1(0)=0.988$ ,  $\Phi_0(0)=0.010$  for an original  $H^-$  beam and at  $\Phi_0(0)=0.995$  for an original  $H^0$  beam. Figure 2 displays

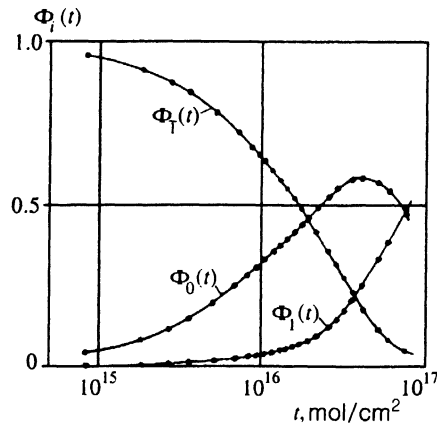


FIG. 2. Measured particle distribution in a beam in terms of the charges as a function of the effective thickness of the  $H_2$  target for original  $H^-$  ions with energy  $E=1.67$  MeV.

the typical behavior of the charge composition of the beam as a function of the thickness of the  $H_2$  target investigated. The cross sections  $\sigma_{10}$ ,  $\sigma_{11}$  were calculated from the measured charge distribution using Eqs. (5) and (6) for the target thicknesses  $t$ , where  $\Phi_0(t)=0.11\text{--}0.20$ , and  $\sigma_{01}$  was calculated using Eq. (4) for  $t$  such that  $\Phi_0(t) \cong 0.60$ . These conditions yielded the most accurate determinations of  $t$ , the fractions  $\Phi_i(t)$ , and ultimately the desired cross sections. The experimental values of the cross section, the neutralization efficiencies  $\Phi_0^{\max}$ , and  $t^{\max}$  found for gaseous targets and incident particle energies  $E=1.67$  and 5.0 MeV, together with the error  $\delta$  in their measurements corresponding to one standard deviation, are compiled in Tables I and II.

For the He, Ar, and  $H_2$  targets the cross sections we measured agreed with the experimental results reported in Refs. 2 and 3 to within experimental error. The sum of the cross sections  $\sigma_{\Sigma}=\sigma_{10}+\sigma_{11}$  for He and  $H_2$  targets is practically the same as the analogous sums calculated in Refs. 9 and 11. If we compare the cross sections  $\sigma_{10}$ ,  $\sigma_{01}$  we obtained with those calculated by Riesselmann *et al.*,<sup>10</sup> we observe that they agree well (for light targets our cross sections are higher by 5–20% than those of Ref. 10, whereas for Kr and Xe they are lower by factors  $\sim 1.2$  and  $\sim 1.4$  respectively).

The experiments with a potassium target were carried out at incident particle energies  $E=5.14$  MeV. The target thickness was determined from the well-known<sup>17,18</sup> dependence of the saturated pressure of K vapor on temperature. The results of the measurements are entered in Table II. The value of  $\Phi_0^{\max}$  which we obtained agrees with that found in Ref. 5. The characteristic scattering angle<sup>11,19</sup> of  $H^0$  atoms when  $H^-$  ions are neutralized in a K target, corresponding to the half-width of the position-angle distribution of  $H^0$  atoms at half maximum, was measured using the equipment and technique described in Ref. 16, and was equal to  $\theta_{1/2}^{(10)}=1.45 \cdot 10^{-5}$  rad  $\pm 10\%$ .

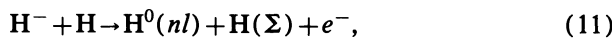
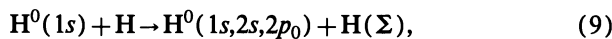
TABLE I. Experimental data for the (01), ( $\bar{1}0$ ), and ( $\bar{1}1$ ) processes in which hydrogen particles with energy  $E=1.67$  MeV interact with various gaseous targets.

Gas	$\sigma_{01}$	$\sigma_{\bar{1}0}$	$\sigma_{\bar{1}1}$	$\Phi_0^{\max}$	$t^{\max}$
He	8.62	29.7	1.20	0.545	63.2
Ar	117	319	19.2	0.518	4.95
Kr	135	328	22.5	0.511	4.60
Xe	170	403	33.9	0.505	2.98
H <sub>2</sub>	11.8	42.7	1.24	0.582	40.8
O <sub>2</sub>	106	274	15.3	0.518	5.80
CO <sub>2</sub>	131	331	17.4	0.528	4.78
C <sub>2</sub> H <sub>2</sub>	-	-	-	0.548	-
$\delta, \%$	7	9	25	1	11

Note: The cross sections are given in units of  $\times 10^{-18}$  cm<sup>2</sup> and the target thickness in units of  $\times 10^{15}$  cm<sup>-2</sup>.

#### 4. CALCULATION OF CROSS SECTIONS FOR H TARGETS

Extending the calculations performed in Ref. 11 for a helium target, we considered the following processes in which hydrogen particles scatter from an H target with and without a change in charge:



Using monatomic hydrogen as the target enables us to obtain simple analytical expressions for the differential and some total cross sections of the processes described by Eqs.

(8)–(12) and to estimate the cross sections for H<sub>2</sub> targets by using the summation principle, according to which the cross section for a given process in which particles interact with a molecule is equal to the sum of the corresponding scattering cross sections for the atoms which make up that molecule. In addition, as will be shown below, collisions which are symmetric in the interacting particles have a number of distinctive features. These include the high efficiency with which H<sup>-</sup> ions are neutralized in molecular hydrogen (58% in the asymptotic ion energy range; see Tables I and II).

Our starting point will be a closed form of the Born approximation<sup>9</sup> (the closure approximation). This takes into account all final states of the H target, including both the discrete and continuous spectrum (this is indicated by the symbol  $\Sigma$  in Eqs. (8)–(12). In this approximation the role of the target in the formation of the differential scat-

TABLE II. Experimental data for the (01), ( $\bar{1}0$ ), and ( $\bar{1}1$ ) processes in which hydrogen particles with energy  $E=5.0$  MeV interact with gaseous targets.

Gas	$\sigma_{01}$	$\sigma_{\bar{1}0}$	$\sigma_{\bar{1}1}$	$\Phi_0^{\max}$	$t^{\max}$
He	4.61	10.9	0.190	0.581 <sup>c</sup>	136 <sup>c</sup>
Ar	60.4	125	4.62	0.495 <sup>c</sup>	11.0 <sup>c</sup>
Kr	66.5	165	8.19	0.524 <sup>c</sup>	8.99 <sup>c</sup>
Xe	105	229	12.0	0.500 <sup>c</sup>	6.10 <sup>c</sup>
H <sub>2</sub>	4.70	15.3	0.287	0.581	117
O <sub>2</sub>	44.0	110	4.01	0.528	13.4
CO <sub>2</sub>	58.2	145	4.56	0.530	10.0
C <sub>2</sub> H <sub>2</sub>	32.8	89.3	2.05	0.544	15.1
$\delta, \%$	6	8	23	1	12
K*	167	387	13.8	0.525	3.20
$\Delta, \%$	10	14	35	1	15

Notes: The cross sections are given in units of  $\times 10^{-18}$  cm<sup>2</sup> and the target thickness in units of  $\times 10^{15}$  cm<sup>-2</sup>. An asterisk (\*) labels the results for a potassium target obtained with energy  $E=5.14$  MeV (here  $\Delta$  is the measurement error for a K target). The subscript (0) signifies that the quantities  $\Phi_0^{\max}$  and  $t^{\max}$  for inert gases were not measured directly but were calculated using Eqs. (7) from the cross sections we measured.

TABLE III. Total cross sections for the scattering of  $H^0$  atoms and  $H^+$  and  $H^-$  ions in atomic hydrogen when electrons are removed and when there is no change in the charge (in units of  $\times 10^{-18}$  cm<sup>2</sup>), calculated in the present work.

$E$ , MeV	$\sigma_{\Sigma}$	$\sigma_{00}$	$\sigma_{00}^{(1s)}$	$\sigma_{00}^{(2s)}$	$\sigma_{00}^{(2p)}$	$\sigma_{i\bar{i}}$	$\sigma_{11}$
0.1	389	71.7	57.2	3.47	11.1	82.3	320
0.15	278	49.4	38.1	2.42	8.82	68.5	237
0.2	215	37.7	28.6	1.85	7.22	59.8	191
0.3	148	25.6	19.1	1.25	5.25	48.9	139
0.4	113	19.4	14.3	0.940	4.11	41.8	111
0.6	76.5	13.0	9.53	0.629	2.86	33.1	79.8
0.71	65.0	11.0	8.05	0.532	2.45	29.8	69.6
0.8	57.8	9.81	7.15	0.472	2.19	27.7	63.04
1	46.5	7.87	5.72	0.378	1.77	23.9	52.40
1.15	40.5	6.85	4.97	0.329	1.55	21.8	46.64
1.67	28.0	4.74	3.42	0.227	1.08	16.9	34.08
2	23.5	3.96	2.86	0.189	0.910	14.9	29.25
3	15.7	2.64	1.91	0.126	0.612	11.1	20.69
5	9.43	1.59	1.14	0.0756	0.369	7.53	13.31
6.9	6.84	1.15	0.829	0.0548	0.268	5.86	10.06
10.4	4.54	0.765	0.550	0.0364	0.179	4.23	7.02
14.9	3.17	0.534	0.384	0.0254	0.125	3.17	5.11
20	2.36	0.398	0.286	0.0189	0.093	2.48	3.94

tering cross section is determined<sup>9,11</sup> by the factor

$$\{S_{inc}^H(\bar{q}) + |F_0^H(\bar{q})|^2\} = \frac{2x(8+x)}{(4+x)^2}, \quad (13)$$

where  $S_{inc}^H$  and  $F_0^H$  are the incoherent scattering function and the elastic form factor of a hydrogen atom, and we have written  $x = (\bar{q}a_0)^2$ , where  $\bar{q}$  is the average value of the wave number corresponding to an average value of the momentum transferred in a collision of  $\Delta\bar{p} = \hbar\bar{q}$  for scattering by the angle  $\theta$  in the laboratory coordinate system and  $a_0$  is the radius of the first Bohr orbit of an H atom. It can easily be shown that with small angles  $\theta$  we have  $x = x_0 + k^2 a_0^2 \theta^2$ , where  $\mathbf{k} = \mathbf{p}/\hbar$  is the wave vector of the incident particle in the laboratory frame and  $x_0 = (\bar{q}_{min} a_0)^2$  is determined following Ref. 9 for  $\theta = 0$ .

As in Ref. 11, the electronic state of the  $H^-$  ion will be described by the Chandrasekar wave function; in the same work the form factors and  $S_{inc}^{H^-}$  functions needed to calculate the cross sections of the processes (9)–(12) are given, by means of which we find the following expression for the differential cross sections of the processes in question:

$$\frac{d\sigma_{11}(\theta)}{d\Omega} = 8a_0^2 \left(\frac{M_p}{m_e}\right)^2 \frac{8+x}{x(4+x)^2}, \quad (14)$$

$$\frac{d\sigma_{00}^{(1s)}(\theta)}{d\Omega} = 8a_0^2 \left(\frac{M_H}{m_e}\right)^2 \frac{x(8+x)^3}{(4+x)^6}, \quad (15)$$

$$\frac{d\sigma_{00}^{(2s)}(\theta)}{d\Omega} = 2^8 a_0^2 \left(\frac{M_H}{m_e}\right)^2 \frac{x(8+x)}{(4+x)^2(2.25+x)^6}, \quad (16)$$

$$\frac{d\sigma_{00}^{(2p)}(\theta)}{d\Omega} = 576a_0^2 \left(\frac{M_H}{m_e}\right)^2 \frac{8+x}{(4+x)^2(2.25+x)^6}, \quad (17)$$

$$\frac{d\sigma_{1\bar{1}}(\theta)}{d\Omega} = 8a_0^2 \left(\frac{M_{H^-}}{m_e}\right)^2 |F_0^{H^-}(x)|^2 \frac{8+x}{x(4+x)^2}, \quad (18)$$

$$\frac{d\sigma_{10}(\theta)}{d\Omega} + \frac{d\sigma_{11}(\theta)}{d\Omega} = 16a_0^2 \left(\frac{M_{H^-}}{m_e}\right)^2 S_{inc}^{H^-}(x) \frac{8+x}{x(4+x)^2}, \quad (19)$$

where  $m_e$ ,  $M_p$ ,  $M_H$ ,  $M_{H^-}$  are the masses of an electron and of the corresponding hydrogen particles.

The differential cross sections (14)–(19) are rapidly decreasing function of  $\theta$ . Hence in calculating the total cross sections it makes sense to carry out the formal integration of these expressions over the semiinfinite interval from  $x_0$  (at  $\theta = 0$ ) to  $\infty$ . For the process (8) we have

$$\sigma_{11} = \frac{4\pi}{k_p^2} \left(\frac{M_p}{m_e}\right)^2 \left[ \ln\left(1 + \frac{4}{x_0}\right) - \frac{2}{4+x_0} \right], \quad (20)$$

where for  $x_0$  we can use the approximate expression  $x_0 = 6.246 \cdot 10^{-3}/E$  (here and in what follows  $E$  is given for convenience in MeV). At  $E = 0.1$  MeV this leads to values of  $x_0$  which are  $\approx 2\%$  less than the exact values; with increasing  $E$  this discrepancy quickly levels out. From Eq. (20) it follows that for  $E > 1$  MeV we have  $\sigma_{11} \sim \ln E/E$ . For the characteristic scattering angles<sup>11</sup> we find from (14) the asymptotic expression (here and below  $\theta$  is measured in radians)

$$\theta_{1/2}^{(11)} = \frac{6.80 \cdot 10^{-6}}{E}, \quad (21)$$

which is smaller by a factor of 2.5 than for scattering by He (Ref. 11).

Integrating (15) we find

TABLE IV. Characteristic scattering angles for hydrogen particles in monatomic hydrogen (in units of  $\times 10^{-6}$  rad), calculated in the present work.

$E$ , MeV	$\theta_{1/2}^{\Sigma}$	$\theta_{1/2}^{(00)}$	$\theta_{1/2}^{(ii)}$	$\theta_{1/2}^{(11)}$
0.1	124.3	285.8	41.43	66.75
0.15	92.04	169.4	30.33	44.75
0.2	76.03	133.6	24.14	33.66
0.3	59.26	102.0	17.33	22.52
0.4	50.17	85.9	13.61	16.92
0.6	40.05	68.4	9.59	11.30
0.71	36.57	62.4	8.26	9.55
0.8	34.30	58.6	7.43	8.48
1	30.47	52.1	6.07	6.79
1.15	28.32	48.3	5.35	5.91
1.67	23.33	39.8	3.78	4.07
2	21.26	36.3	3.19	3.40
3	17.28	29.5	2.17	2.27
5	13.34	22.8	1.33	1.36
6.9	11.34	19.4	0.966	0.986
10.4	9.23	15.8	0.646	0.654
14.9	7.70	13.2	0.452	0.457
20	6.65	11.4	0.338	0.340

$$\sigma_{00}^{(1s)} = \frac{1.6\pi}{k_H^2} \left( \frac{M_H}{m_e} \right)^2 \left[ \frac{2(8+x_0)^2(x_0^2+7x_0+4)}{(4+x_0)^5} + \frac{3(6+x_0)}{(4+x_0)^2} \right], \quad (22)$$

where  $x_0$  is determined in the same way as above. The integration of Eqs. (16) and (17) is elementary, but it yields expressions containing many terms. For this reason we write down the asymptotic expressions for the processes (9), obtained from the exact formulas by substituting  $x_0=0$  (in units of  $10^{-18}$  cm<sup>2</sup>):

$$\sigma_{00}^{(1s)} = \frac{5.72}{E}, \quad \sigma_{00}^{(2s)} = \frac{0.381}{E},$$

$$\sigma_{00}^{(2p)} = \frac{1.86}{E}, \quad \sigma_{00} = \frac{7.96}{E}, \quad (23)$$

where  $\sigma_{00} = \sigma_{00}^{(1s)} + \sigma_{00}^{(2s)} + \sigma_{00}^{(2p)}$ . The characteristic angle for the process (9) in which hydrogen atoms are formed in the 1s state is

$$\theta_{1/2}^{(00)}(1s) = 1.29 \cdot 10^{-4} E^{1/2}. \quad (24)$$

Exact values of the calculated cross sections and characteristic angles for the processes in question are assembled in Tables III and IV. Comparing the results of the calculations for monatomic hydrogen targets and for helium targets,<sup>11</sup> we can draw the following conclusions:

1. For (11) collisions the ratio  $\sigma_{11}/\sigma_{\Sigma}$  for an H target is higher in the energy range in question by a factor of 1.2–1.6, while the characteristic angle  $\theta_{1/2}^{(11)}$  is smaller by a factor of  $\approx 2.5$ .

2. When we go from He to H the ratio  $\sigma_{00}^{(2p)}/\sigma_{00}$  increases by a factor of 1.7–4, as a result of which the characteristic angle for (00) collisions becomes largely determined by the process of formation of hydrogen atoms in

the 2p state. Ultimately the value of  $\theta_{1/2}^{(00)}$  for an H target is reduced by a factor 1.7–3.6. The value of  $\sigma_{00}/\sigma_{\Sigma}$  for hydrogen is smaller by a factor 1.3–1.9.

3. In the range  $E \geq 0.2$  MeV the ratio  $\sigma_{\bar{1}\bar{1}}/\sigma_{\Sigma}$  in hydrogen is larger by a factor 1.2–1.8 than in He, while the  $\sigma_{1/2}^{(\bar{1}\bar{1})}$  angles are reduced by a factor of 1.7–2.5.

Thus, the characteristic angles for scattering processes involving hydrogen particles where no change in charge occurs and the values of  $\sigma_{00}/\sigma_{\Sigma}$  are considerably reduced for an H target, especially for large values of  $E$ . The angle  $\theta_{1/2}^{(\bar{1}\bar{0})}$  is also smaller (by  $\approx 10\%$  at energies  $E=5$ –20 MeV), while the ratio  $\theta_{1/2}^{(00)}/\theta_{1/2}^{(\bar{1}\bar{0})}$  has decreased by a factor  $\approx 2.8$ . This implies that a hydrogen target is more effective from the standpoint of forming beams of hydrogen atoms with the smallest possible angular divergence in the process of neutralizing  $H^-$  ions for  $t \approx t^{\max}$ , and similarly for proton beams.

The characteristic angles and cross sections vary as functions of the energy of the incident particles for  $E \geq 1$  MeV as follows [here and below the quantities distinguished by the subscript  $\Sigma$  refer to the process  $(\bar{1}\bar{0}) + (\bar{1}\bar{1})$ ]:  $\theta_{1/2}^{\Sigma} \propto E^{-1/2}$ ,  $\theta_{1/2}^{(00)} \propto E^{-1/2}$ ,  $\theta_{1/2}^{(\bar{1}\bar{1})} \propto E^{-1}$ ,  $\sigma_{\Sigma} \propto E^{-1}$ ,  $\sigma_{\bar{1}\bar{1}} \propto E^{-0.75}$ , which agrees with the results for He (Ref. 11), and for  $\sigma_{\Sigma}$  and H targets with the results of Refs. 7, 9, and 10. The angular dependence is identical for the differential cross sections (8)–(12) in H and He targets. The location of the angle  $\theta_0$  for which  $d\sigma_{\bar{1}\bar{1}}(\theta_0)/d\Omega = 0$ , holds is the same for both targets, since it is determined by the vanishing of the form factor  $F_0^{H^-}$  [cf. Eq. (18) and Ref. 11].

The values of the cross section  $\sigma_{\Sigma}$  calculated in this work in the energy range  $E=0.1$ –20 MeV exceed the cross sections obtained theoretically by Lee and Chen<sup>9</sup> by 15%,

those obtained by Gillespie<sup>7</sup> by 15%, and those obtained by Riesselmann *et al.*<sup>10</sup> by 30%; but they are smaller than the cross sections calculated by Radchenko<sup>19</sup> by 0–35% (depending on  $E$ ). The experimental results<sup>6</sup> for  $\sigma_{10}$  cross sections and  $E=0.1-0.3$  MeV are smaller than our cross sections by  $\approx 25\%$ .

In Refs. 10 and 20 it was shown that for  $E \geq 1$  MeV the additivity principle for (01), (10) processes of scattering by  $H^-$ ,  $H_2$  targets is satisfied to high accuracy. This enables us to compare the cross sections  $\sigma_{\Sigma}$  from Table III which we have calculated, applied to  $H_2$  targets (by multiplying by a factor 2) with our experimental data for  $\sigma_{10} + \sigma_{11}$  given in Tables I and II. The theoretical values exceed the measured values by 15–20%.

## 5. SCATTERING BY MODEL POTENTIALS

### 5.1. Scattering by the Thomas–Fermi potential

The systematic application of the Born approximation for complex targets encounters serious difficulties of a computational nature, which can be circumvented by introducing some sort of simplifying assumptions. In the Born approximation in the approach of Ref. 9, invoking a model for the potential of the colliding particles, we can seek an expression for the differential scattering cross section of any process in a general form and thereby attempt to extract the basic behavior of interactions of the form (8)–(12) for more complicated targets. With this aim we use the Thomas–Fermi potential approximation for the Teitz function,  $\varphi(x) = (1+cx)^{-2}$ , where  $c$  is the Teitz constant, the argument is  $x = 1.12956cZ_2^{1/3}R/a_0$ , and  $R$  is the distance between the nucleus of the scattering atom with charge  $Z_2$  at the point at which the value of the potential is determined. Neglecting the changes in the Thomas–Fermi statistical field resulting from the presence of the incident particle we find for the processes in question in the center-of-mass system the formula

$$\frac{d\sigma_{\alpha_f\alpha_i}(\nu)}{d\Omega} = \frac{M^2 e^4 Z_2^2 k_f}{4\pi^2 \hbar^4 k_i} \left| \iint \left[ \frac{Z_1}{R(1+\alpha R)^2} - \sum_{a=1}^{Z_e} \frac{1}{|\mathbf{R}+\mathbf{r}_a| (1+\alpha|\mathbf{R}+\mathbf{r}_a|)^2} \right] \times e^{-i\mathbf{q}\mathbf{R}} \Psi_{\alpha_f}^* \Psi_{\alpha_i} dV d\tau \right|^2, \quad (25)$$

where  $\nu$  is the scattering angle,  $M$  is the reduced mass of the colliding particles, and  $e$  is the elementary charge;  $\mathbf{k}_i$  and  $\mathbf{k}_f$  are the wave vectors corresponding to the motion of a particle with reduced mass  $M$  and the velocity of the incident particle  $A$  before and after the collision,  $\mathbf{q} = \mathbf{k}_f - \mathbf{k}_i$ ;  $Z_1$ ,  $Z_e^A$  are the charge of the nucleus in units of  $e$  and the number of electrons of the incident system  $A$ ;  $\alpha = 1.12956cZ_2^{1/3}/a_0$ ,  $\Psi_{\alpha_i}$ ,  $\Psi_{\alpha_f}$  are the wave functions of the  $A$  system before and after the collision;  $R$  is the radial distance between the  $A$  particle and the nucleus of a target atom;  $dV$  is the volume element corresponding to the radius  $\mathbf{R}$ ;  $\mathbf{r}_a$  is the radius vector of the  $a$ th electron of the  $A$

particle with respect to its nucleus; and  $d\tau$  is an element of the configuration space of the  $Z_e^A$  electrons of the incident particle.

Integration of (25) over  $dV$  reduces to the following integral, whose value can be easily shown to be expressible in terms of the integral sine and cosine functions

$$\int \frac{e^{-i\mathbf{q}\mathbf{R}} dV}{R(1+\alpha R)^2} = \frac{4\pi}{\alpha^2} \left\{ \sin \frac{q}{\alpha} \left[ \frac{\pi}{2} - \text{Si} \left( \frac{q}{\alpha} \right) \right] - \cos \frac{q}{\alpha} \text{Ci} \left( \frac{q}{\alpha} \right) \right\}. \quad (26)$$

Substituting (26) in (25) we find

$$\frac{d\sigma_{\alpha_f\alpha_i}(\nu)}{d\Omega} = \frac{4M^2 e^4 Z_2^2 k_f}{\hbar^4 \alpha^4 k_i} \left\{ \sin \frac{q}{\alpha} \left[ \frac{\pi}{2} - \text{Si} \left( \frac{q}{\alpha} \right) \right] - \cos \frac{q}{\alpha} \text{Ci} \left( \frac{q}{\alpha} \right) \right\}^2 |F_{\alpha_f\alpha_i}^A(q)|^2, \quad (27)$$

where  $F_{\alpha_f\alpha_i}^A$  is the form factor of the particle  $A$ . For large values of  $q/\alpha$  for the expression which appears in braces in Eqs. (26) and (27) we can use the expansion

$$\{ \dots \} = \left( \frac{\alpha}{q} \right)^2 - 6 \left( \frac{\alpha}{q} \right)^4 + O, \quad (28)$$

where  $O$  represents a small quantity of higher order. Then for the bare  $A$  nuclei, retaining the first term in the expansion (28) and noting that we have  $q = 2k_i \sin(\nu/2)$ , we obtain the Rutherford formula from Eq. (27). We determine the angle  $\nu_R$  above which the relation (27) for bare  $A$  nuclei yields the Rutherford formula from the condition under which the second term in the expansion (28) is smaller than the first by a factor  $10^{-2}$ . Thus we obtain

$$\sin \frac{\nu_R}{2} = \frac{13.8cZ_2^{1/3}}{k_i a_0} = 7.1 \frac{Z_2^{1/3}}{k_i a_0} \quad (29)$$

(we use  $c=0.5125$  for the value of the Teitz constant).

At distances greater than an atomic radius the Thomas–Fermi potential is substantially larger than the true value; the Teitz approximation accentuates this discrepancy. It is just at these energies that hydrogen particles interact with target atoms in processes of the form (8)–(12) for scattering through angles  $\theta < (2-3)\theta_{1/2}$ . Expression (27) is therefore valid and its use is meaningful for the range of scattering angles from  $(3-5)\theta_{1/2}$  to  $\theta_R$  (the angle  $\theta_R$  corresponds to the angle  $\nu_R$  in the laboratory coordinate frame). A more precise value for the lower boundary of this range could reasonably be established by comparison with experimental data. Calculations of the differential cross sections for scattering through large angles are interesting, in particular, in connection with the study of the “halo” of tightly collimated beams of fast hydrogen particles.

In order to illustrate the above remarks we use (27) to calculate the characteristic angles and total cross sections in the process in which bare nuclei are scattered by atoms with no change in the charge. We find [cf. Eq. (21)] that the characteristic angle is given by

$$\theta_{1/2} = 6.25 \cdot 10^{-6} Z_2^{1/3} A^{-1} (E_A/A)^{-1/2}, \quad (30)$$

where  $E_A/A$  is the energy in the laboratory coordinate system of the  $A$  nucleus in MeV/nucleon and the cross section (in  $\text{cm}^2$ ) is

$$\sigma = 1.91 \cdot 10^{-17} Z_1^2 Z_2^{A/3} (E_A/A)^{-1}. \quad (31)$$

For protons expression (31) yields values larger by a factor of 3–7 than the experimental cross sections of Refs. 11 and 14. The dependence on  $Z_1$  and  $Z_2$  in (31) is also too strong.

It is clear that as the energy  $E_A$  increases an interaction process involving colliding particles will be characterized by smaller and smaller impact parameters, i.e., there will be an increase in the fraction of collisions which take place in the region of the space where the Thomas–Fermi potential correctly describes the potential of the target atom. Consequently, Eq. (27) will show better agreement with experiment.

## 5.2. Scattering by a dipole potential in the instantaneous dipole moment approximation

We are interested in the scattering of hydrogen particles through small angles, corresponding to large impact parameters. If the total charge of the scattering system with dipole moment  $\mathbf{d}$  is equal to zero, then the potential energy of the incident  $A$  particle in the dipole field at large distances can be represented in the form

$$U = e\mathbf{d} \left( Z_1 \frac{\mathbf{R}}{R^3} - \sum_{a=1}^{Z_2} \frac{\mathbf{R} + \mathbf{r}_a}{|\mathbf{R} + \mathbf{r}_a|^3} \right) = e\mathbf{d}\mathbf{K}. \quad (32)$$

Using (32) we find in analogy with (25) in the center-of-mass coordinate system

$$\frac{d\sigma_{\alpha_f \alpha_i}^{\mathbf{d}}(\nu)}{d\Omega} = C |\mathbf{d}\mathbf{M}|^2, \quad (33)$$

where  $C = (M^2 e^2 / 4\pi^2 \hbar^4) (k_f/k_i)$ ,  $\mathbf{M} = \langle \Psi_{\alpha_f} | \mathbf{K} e^{-i\mathbf{q}\mathbf{R}} | \Psi_{\alpha_i} \rangle$ . We average (33) over the directions of the vector  $\mathbf{d}$  to obtain

$$\frac{d\sigma_{\alpha_f \alpha_i}(\nu)}{d\Omega} = \frac{1}{4\pi} \int \frac{d\sigma_{\alpha_f \alpha_i}^{\mathbf{d}}(\nu)}{d\Omega} d\Omega = \frac{C}{3} d^2 |\mathbf{M}|^2. \quad (34)$$

Since the formula for the vector matrix element  $\mathbf{M}$  contains an integral over  $dV$ , its evaluation reduces to an integral which can be shown to be equal to

$$\int \frac{\mathbf{R}}{R^3} e^{-i\mathbf{q}\mathbf{R}} dV = -\frac{4\pi i}{q^2} \mathbf{q}. \quad (35)$$

Using (35) we find that  $\mathbf{M}$  is expressed in terms of the form factor of the  $A$  system:

$$\mathbf{M} = -\frac{4\pi i}{q^2} \mathbf{q} F_{\alpha_f \alpha_i}^A(\mathbf{q}). \quad (36)$$

Substituting (36) in (34) we find for the differential scattering cross section in the laboratory coordinate frame

$$\frac{d\sigma_{\alpha_f \alpha_i}(\theta)}{d\Omega} = \frac{4a_0^2}{3(qa_0)^2} \left( \frac{M_A}{m_e} \right)^2 \left( \frac{d}{ea_0} \right)^2 \frac{k_f}{k_i} |F_{\alpha_f \alpha_i}^A(\mathbf{q})|^2. \quad (37)$$

After summing (37) over  $\alpha_f \neq \alpha_i$  we arrive at a formula which differs from (37) in having  $Z_e^A S_{\text{inc}}^A(\bar{q})$  for incoherent scattering of the  $A$  particle in place of  $|F_{\alpha_f \alpha_i}^A(\mathbf{q})|^2$ . These relations will obviously be useful in studying processes involving scattering through small angles in interactions with targets having a large dipole moment, such as molecules of alkaline–halide compounds.

Relation (37) can be used to carry out calculations of the differential cross sections for scattering of particles in different processes, using the concept of the average value of the “instantaneous dipole moment” (IDM) of the target atom  $B$ . Specifically, assume that the velocity of the incident particle is much larger than the velocity of the orbital electrons of the  $B$  atom, so that during the time of the collision the locations of these electrons remains essentially unchanged (using the corpuscular approach). The instantaneous position of the electrons, specified by the vectors  $\mathbf{r}_i$ , corresponds to a value of the IDM  $|\mathbf{d}| = e(\sum_{i,j=1}^{Z_2} \mathbf{r}_i \mathbf{r}_j)^{1/2}$ . Averaging  $|\mathbf{d}|$  over an ensemble of target atoms we find the average value of the IDM:

$$d = e \int \left( \sum_{i,j=1}^{Z_2} \mathbf{r}_i \mathbf{r}_j \right)^{1/2} |\Psi_B(\mathbf{r}_1, \dots, \mathbf{r}_{Z_2})|^2 d\tau_B, \quad (38)$$

where  $\Psi_B$  is the wave function of the  $B$  atom and  $d\tau_B$  is an element of the configuration space of the  $Z_2$  electrons of the  $B$  atom. Using the ergodic theorem we find that the concept of the IDM and Eq. (38) continue to apply even for small incident particle velocities. However, at small velocities the collisions can cause considerable distortion of the electronic states of the target owing to the presence of the incident particle. Generally speaking, these result in theoretical cross sections which exceed the actual values. In what follows we will refer to the theoretical model based on Eqs. (37) and (38) as the IDM approximation.

Let us consider a target in the form of a hydrogen atom  $H(nl)$ . In this case the integral in Eq. (38) is the average radius of an atomic electron in the  $nl$  state, given by<sup>22</sup>  $\bar{r} = 0.5[3n^2 - l(l+1)]a_0$ . For a hydrogen atom in the ground state we have  $d = 1.5ea_0$ . Substituting this value of the IDM in (37) and integrating with respect to  $\Omega$ , we find for the processes (9) in which fast H atoms form in the  $2s$  and  $2p_0$  states the cross sections [in units of  $10^{-18} \text{cm}^2$ ; cf. Eq. (23)]

$$\sigma_{00}^{(2s)} = \frac{0.414}{E}, \quad \sigma_{00}^{(2p)} = \frac{1.65}{E}. \quad (39)$$

The cross section  $\sigma_{00}^{(1s)}$  in the IDM approximation, however, is larger than the “exact” cross section given by (23) by a factor of ten, since the corresponding differential cross section (37) falls off as a function of  $\theta$  too slowly (the integral for  $\sigma_{00}^{(1s)}$  diverges in the formal limit  $\theta \rightarrow \infty$ ). In the final analysis this is related to the behavior of the interaction potential (32) at small distances. Thus, in order to apply the IDM approximation successfully at large values of  $\theta$  it is necessary to correct the potential (32) at small distances and (or) to perform calculations for processes

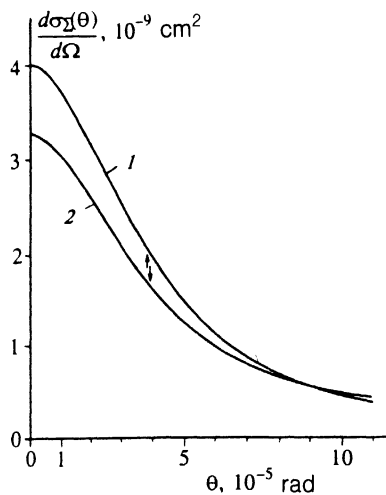


FIG. 3. Differential cross section for scattering of particles by monatomic hydrogen for the  $(\bar{1}0) + (\bar{1}1)$  process in which electrons are lost by the  $H^-$  ions with energy  $E=0.71$  MeV, calculated from the "exact" formula (19), trace 1, and in the IMD approximation, trace 2. For each trace the arrows indicate the location of the angle corresponding to the half maximum of the differential cross section for  $\theta=0$ .

such that the differential cross section (37) falls off at large  $\theta$  at least as fast as  $(qa_0)^{-2}$ . This last condition holds for the cross section (39).

Since Eq. (32) correctly describes the potential for the interaction of a particle with a dipole at large distances, relation (37) in the IDM approximation is found to hold for small scattering angles. As an example, Fig. 3 shows the differential cross section for scattering of  $H^-$  ions by monatomic hydrogen in the  $(\bar{1}0) + (\bar{1}1)$ , process, calculated according to the "exact" expression (19) and using Eq. (37) in the IDM approximation. Such good agreement in the differential cross sections for small values of  $\theta$  suggests that the IDM approximation is promising. This also applies to processes in which the differential cross section in the IDM approximation decreases as  $q^{-2}$  when  $q$  increases without limit.

In fact, the differential cross section for scattering of particles by complex atoms can be derived over the whole range of angles  $\theta$  by "matching" Eq. (27), which is valid for large  $\theta$ , with Eq. (37) for small  $\theta$  (using the IDM approximation for the electrons of the outer shell of the atom) at the point where Eqs. (27) and (37) coincide. We retain the designation "IDM approximation" for this approach since the calculations reveal that the main contribution to the resulting total cross sections for these processes comes from Eq. (37) for the scattering by the dipole potential.

Evaluation of the IDM for inert gas atoms is a separate problem, so in the present work we have calculated the characteristic angles and cross sections for the processes  $(\bar{1}0) + (\bar{1}1)$ ,  $(\bar{1}\bar{1})$ ,  $(00)$ ,  $(11)$  for atoms of the alkaline metals (Li, Na, K, Rb, Cs). Their IDM is determined by assuming that the atomic core is pointlike and has a charge  $+e$ . In this case the absolute value of the IDM is equal to the product  $d=e\langle r \rangle$  of the elementary charge by the aver-

age radius of a valence electron, in accordance with Eq. (38).

The magnitudes of the minimum momentum transfer in a collision, which are needed in calculations of processes in which particles are scattered without change in charge in the closed form of the Born approximation (cf. Sec. 3 and Refs. 9 and 11), as in the work of Meyerhof *et al.*,<sup>21</sup> are determined according to the expression

$$\bar{q}_{\min} \hbar v = I + \Delta E(nl), \quad (40)$$

where  $v$  is the velocity of the incident particle,  $I$  is the ionization potential of a target particle, and  $\Delta E(nl)$  is the excitation energy of the incident particle. The values of  $\langle r \rangle$  and  $I$  were taken from Radzig and Smirnov.<sup>23</sup>

We also carried out similar calculations for the following diatomic alkaline-halide molecular compounds: NaCl, KCl, KBr, KI, and CsI. For the magnitude of the quantity  $d$  in the calculations of the differential cross sections for scattering through small angles according to Eq. (37) we used the average values of the intrinsic electric dipole moments of the molecules. The magnitudes of the dipole moments, and also the molecular ionization potentials which enter in the relation (40), are noted in Ref. 24. Scattering through large angles is described by the sum of the differential cross sections (27) for the individual atoms that make up the molecules. Then the differential cross sections obtained for large and small  $\theta$  are matched at the intersection point.

The tables containing the results of the actual calculations for all the targets listed above at  $E=0.1-20$  MeV are excessively detailed. Therefore, without losing much of the accuracy of the calculations, we represent the characteristic angles and cross sections for these scattering processes by their asymptotic expressions:

$$\theta_{1/2}^{\Sigma}, \theta_{1/2}^{(00)} = \frac{k_{ij}}{E^{1/2}}, \quad \theta_{1/2}^{(\bar{1}\bar{1})} = \frac{k_{\bar{1}\bar{1}}}{E}, \quad \theta_{1/2}^{(11)} = \frac{k_{11}}{E}, \quad (41)$$

$$\sigma_{\Sigma}, \sigma_{00} = \frac{c_{ij}}{E}, \quad \sigma_{\bar{1}\bar{1}} = \frac{c_{\bar{1}\bar{1}}}{E^n}, \quad \sigma_{11} = c_{11} \frac{\ln(E/a)}{E}. \quad (42)$$

The parameters which appear in these relations are given in Table V. They have numerical values such that when substituted in Eqs. (41) and (42) they yield angles in units of  $\mu\text{rad}$  and cross sections in units of  $10^{-18} \text{ cm}^2$  if  $E$  is measured in MeV.

In the asymptotic energy range  $E \gg 1$  MeV the angles (41) and cross sections (42) are essentially the same as the results of the actual calculations for arbitrary processes (generally speaking, the difference is less than 1%). As the energy decreases the difference between them grows noticeably for some quantities. At  $E=0.1$  MeV the calculated values of  $\theta_{1/2}^{(\bar{1}\bar{1})}$  are less than the asymptotic values by 10-30% (depending on the target); those of  $\sigma_{00}(2p)$  are less than the asymptotic values by 15-30%; and those of  $\sigma_{\bar{1}\bar{1}}$  are less than the asymptotic values by 3-15%. For the other quantities the difference is  $\leq 3\%$ .

Table V also contains the results of calculations in our approximation for H and Li targets, although the application of Eq. (27), which is based on the Thomas-Fermi

TABLE V. Values of the parameters used in Eqs. (41) and (42) for the characteristic angles and the cross sections for the processes  $(\bar{10}) + (\bar{11})$ , (00),  $(\bar{1}\bar{1})$ , (11), evaluated in the IMD approximation for targets consisting of H atoms, alkaline metal atoms, and alkaline-halide molecules.

Process	Parameter	Target										
		H	Li	Na	K	Rb	Cs	NaCl	KCl	KBr	KJ	CsJ
$(10) + (\bar{11})$	$k_{\Sigma}$	32.4	32.4	32.4	32.4	32.4	32.4	32.4	32.4	32.4	32.4	32.4
	$c_{\Sigma}$	42.5	364	535	958	1362	1848	519	456	638	706	907
(00)	$k_{00}$	195	195	195	195	195	195	195	195	195	195	195
	$c_{00}$	11.3	89.8	139	276	447	630	167	155	224	256	334
	$c_{00}(1s)$	9.2	76.0	123	251	418	594	156	146	213	244	319
	$c_{00}(2s)$	0.414	2.76	3.25	5.06	5.83	7.3	2.29	1.82	2.35	2.41	2.96
	$c_{00}(2p)$	1.65	11.0	13.0	20.2	23.3	29.1	9.14	7.27	9.39	9.60	11.8
$(\bar{1}\bar{1})$	$k_{\bar{1}\bar{1}}$	6.76	2.70	2.56	2.17	2.09	1.94	4.44	4.32	3.92	3.67	3.61
	$c_{\bar{1}\bar{1}}$	19.9	251	329	599	826	1121	261	231	331	369	475
	$n$	0.76	0.85	0.87	0.88	0.90	0.91	0.88	0.89	0.90	0.907	0.91
(11)	$k_{11}$	6.80	2.70	2.57	2.17	2.09	1.95	4.46	4.34	3.93	3.68	3.63
	$c_{11}$	6.60	44.08	52.03	81.08	92.98	116.2	36.57	29.10	37.57	38.48	47.34
	$a$	1313.5	80.6	26.0	8.86	1.92	0.893	11.2	4.98	2.11	0.957	0.623

Note. The quantity  $a$  is given in units of  $\times 10^{-6}$  MeV.

potential, is not legitimate in this case. This comment does not apply to the  $\sigma_{00}(2s)$  and  $\sigma_{00}(2p)$  cross sections, since Eq. (27) was not used when they were evaluated in the IMD approximation. The calculations for H and Li targets were performed using the technique of pseudointersection for the curves (27) and (37) (formally they do not intersect for these targets). In this technique the charge  $Z_2$  in Eq. (27) is assigned a value such that the curves are tangent to one another (i.e., pseudointersection occurs). The results obtained for these targets make it possible to compare the calculations in the IMD approximation with the exact calculations for H targets carried out in Sec. 4 of the present work. When we make this comparison we see that the  $\sigma_{00}(2s)$  and  $\sigma_{00}(2p)$  cross sections in the IMD approximation differ by factors of at most  $\approx 1.1$  and  $\approx 0.9$  respectively from the exact values (Table III), while the  $\sigma_{00}(1s)$  cross section is too high by a factor of 1.6. Notable agreement is observed for the cross sections of the processes  $(\bar{10}) + (\bar{11})$ ,  $(\bar{1}\bar{1})$ , (11). In the asymptotic range of  $E$  the  $\sigma_{\Sigma}$  cross sections in the IMD approximation are less than the benchmark calculations by at most 10%, while the  $\sigma_{\bar{1}\bar{1}}$  and  $\sigma_{11}$  cross sections in the IMD approximation are 2–20% low for all  $E$ . As for the characteristic scattering angles,  $\theta_{1/2}^{(\bar{10})}$  in the IMD approximation for  $E \gg 1$  MeV is larger than the angles in Table IV by  $\approx 10\%$  and  $\theta_{1/2}^{(00)}$  is larger than the values in Table IV by a factor of 2–4. The angles  $\theta_{1/2}^{(\bar{1}\bar{1})}$ ,  $\theta_{1/2}^{(11)}$  in the approaches which we are comparing are in essentially total agreement (the discrepancy is less than 1.9%). It is important to note that the behavior of the cross sections and characteristic angles as a function of  $E$  in the IMD approximation is the same as in the exact calculations.

For an Li target the  $\sigma_{00}(2s)$ ,  $\sigma_{00}(2p)$  cross sections in the IMD approximation are lower by a factor 1.3–1.5 calculated in Ref. 12 and exceed the cross sections calculated in Ref. 13 by a similar amount. The energy dependence of these cross sections is the same as in Ref. 12: asymptoti-

cally we have  $\sigma_{00}(2s) \propto E^{-1}$  and  $\sigma_{00}(2p) \propto \ln E/E$  in the range  $E=0.1-1$  MeV. For  $E \gg 1$  MeV we have  $\sigma_{00}(2p) \propto E^{-1}$  [cf. Eq. (42)].

In the energy range  $E=0.1-0.2$  MeV the values of the  $\sigma_{\Sigma}$  cross sections which we calculated for the heavier alkaline metal atoms exceed the experimental data<sup>5</sup> by a factor of 3–7. As already noted, this is related to the fact that as  $E$  decreases the IMD approximation yields an asymptotic upper bound on the cross sections, which does not take into account the distortion of the target due to the colliding particles. The  $\sigma_{\bar{10}}$  cross section which we measured for a potassium target (Table II) is larger than the calculated value (Table V) by a factor of 2.

A noteworthy feature of these calculations is that the cross sections of all the processes in which interaction with alkaline-halide molecules occurs are found to be less than the cross sections for the atoms of the corresponding alkaline metals. The reason for this is that the IMD of the atoms is larger than the dipole moment of the corresponding molecules. Without doubt this assertion is in sharp conflict with the additivity principle and requires experimental verification.

## 6. CONCLUSION

1. The results of the present work permit us to assume that targets consisting of molecules in which hydrogen atoms occupy an essentially peripheral position are close in their properties to targets made of monatomic and molecular hydrogen. In order to test this assumption in the present work we determined the efficiency with which  $H^-$  ions with energy  $E=1.67$  and 5.0 MeV were neutralized in  $C_2H_2$  (the geometric structure of the molecule is H–C–C–H). It was found to be equal to  $\Phi_0^{\max} = 54.8\%$  (see Tables I and II).

2. Comparison of the theoretical values of  $\theta_{1/2}^{(\bar{10})}$  for hydrogen and helium targets (Table IV and Refs. 9 and

11) and the experimental results obtained in the present work for a potassium target, and also Eqs. (27) and (37) and the calculations in the IMD approximation, reinforces the conclusions of Refs. 8 and 15, where it was found that the characteristic angle  $\theta_{1/2}^{(10)}$  depends weakly on the form of the target. As noted in the Introduction, there are no experimental data on this matter for  $E \geq 0.5$  MeV.

3. The calculations performed in the present work and in Ref. 11 for a broad range of targets and processes, and also the experimental results for  $(\bar{1}0)$ ,  $(\bar{1}1)$ ,  $(01)$  processes reveal that the ratios of these cross sections (e.g.,  $\sigma_{00}/\sigma_{\bar{1}0}$ ,  $\sigma_{00}(nl)/\sigma_{00}$ , etc.) change relatively smoothly and to a limited extent as we go from one target to another. Thus, the ratio  $\sigma_{00}(2p)/\sigma_{00}(2s)$  (say) is equal to 4.7 for an H target and 4.0 for the atoms of alkaline metals. We can assume that these ratios of cross sections will vary with some regularity (though not very much) within a single class of targets and will change abruptly when we go from one class of targets to another. An example of this is the discontinuous change in the ratio  $\sigma_{\bar{1}0}/\sigma_{01}$  when we go from gaseous targets to plasma targets. The same thing should be expected when we go to amorphous or monocrystalline film targets.

4. The numerical calculations reveal that for all targets and processes the fraction of particles scattered through angles  $\theta \geq 10\theta_{1/2}$  generally amounts to 10–40%, which underlines the importance of the beam halo problem.

5. Using (36) we reduce the differential cross section (33) in the laboratory coordinate system to the form

$$\frac{d\sigma_{\alpha_f \alpha_i}^d(\theta)}{d\Omega} = 4 \left( \frac{M_A}{m_e} \right)^2 \left( \frac{d}{ea_0} \right)^2 \frac{k_f}{k_i} |F_{\alpha_f \alpha_i}^A(\mathbf{q})|^2 \frac{\cos^2 \gamma}{q^2}, \quad (43)$$

where  $\gamma$  is the angle between the vectors  $\mathbf{d}$  and  $\mathbf{q}$ . It is obvious that the scattering in targets polarized with respect to the orientation of the vector  $\mathbf{d}$  is a minimum in the direction perpendicular to  $\mathbf{d}$ . If we assume that the vector  $\mathbf{d}$  is parallel to the beam axis then it is easy to show that

$$q \cos \gamma = q_{\min} + k_A \frac{M_A}{2M} \theta^2. \quad (44)$$

For scattering angles  $\theta < 10\theta_{1/2}$  the second term in (44) can be neglected. In this case the angular dependence (43) is determined mainly by the factor  $q^{-4}$ , which causes the angular profile of the scattered particles to narrow and also reduces the beam halo relative to other targets. Using (43) we can easily analyze other effects that occur when the

direction of target polarization relative to the beam axis is changed. However, observation of these effects is somewhat hindered due to the precession of the vector  $\mathbf{d}$  about the direction of polarization. Consequently, polarization effects are exhibited most clearly in targets at reduced temperature and large values of the dipole moment.

I wish to express my deep gratitude to B. V. Shul'gin for supporting this work, and to G. D. Ved'manov, Yu. G. Lazarev, Yu. R. Yakovlev, and many others for help in processing and performing the measurements.

<sup>1</sup>H. S. W. Massey, *Negative Ions*, Cambridge Univ. Press (1976).

<sup>2</sup>N. V. Fedorenko, Zh. Tekh. Fiz. **40**, 2481 (1970) [Sov. Phys. Tech. Phys. **15**, 1947 (1971)].

<sup>3</sup>J. S. Risley, Electron. and Atom. Collisions, *Proc. 11th Int. Conf. (Kyoto, 1979)*, Invit. Pap. and Progr. Repts., Amsterdam, etc. (1980), p. 619.

<sup>4</sup>H. Tawara and A. Russek, Rev. Mod. Phys. **45**, 178 (1973).

<sup>5</sup>C. J. Anderson, R. J. Girmius, A. M. Howald, and L. W. Anderson, Phys. Rev. A **22**, 822 (1980).

<sup>6</sup>J. Geddes, J. Hill, M. B. Shah *et al.*, J. Phys. B **13**, 319 (1980).

<sup>7</sup>G. H. Gillespie, Phys. Rev. A **15**, 563 (1977).

<sup>8</sup>J. A. Johnstone, NIM Phys. Res. B **52**, 1 (1990).

<sup>9</sup>Y. T. Lee and J. C. Y. Chen, Phys. Rev. A **19**, 526 (1979).

<sup>10</sup>K. Riesselmann, L. W. Anderson, L. Durand, and C. J. Anderson, Phys. Rev. A **43**, 5934 (1991).

<sup>11</sup>V. I. Radchenko, Zh. Eksp. Teor. Fiz. **103**, 40 (1993) [Sov. Phys. JETP **76**, 22 (1993)].

<sup>12</sup>K. C. Mathur, A. N. Tripathi, and S. K. Joshi, Phys. Rev. A **6**, 1248 (1972).

<sup>13</sup>I. M. Cheshire and H. L. Kyle, Phys. Letters **17**, 115 (1965).

<sup>14</sup>V. I. Radchenko, Zh. Tekh. Fiz. **63**, 200 (1993) [Sov. Phys. Tech. Phys. **38**, 260 (1993)].

<sup>15</sup>B. A. D'yachkov, V. I. Zinenko, and G. V. Kazantsev, Zh. Tekh. Fiz. **47**, 416 (1977) [Sov. Phys. Tech. Phys. **22**, 245 (1977)].

<sup>16</sup>G. D. Ved'manov, V. P. Kozlov, V. N. Kudryavtsev *et al.*, Prib. Teor. Éksp. No. 2, 47 (1989).

<sup>17</sup>É. E. Shpil'rain, K. A. Yaimouch, T. N. Mel'nikova, and A. Ya Polishchuk, *Thermophysical Properties of Lithium Hydride, Deuteride, Tritide, and Their Solutions with Lithium*, AIP, New York (1987).

<sup>18</sup>A. G. Mozgovoï, I. I. Novikov, M. A. Pokrasin *et al.*, in *Reviews of Thermophysical Properties of Materials* [in Russian], No. 151, IVTAN, Moscow (1985).

<sup>19</sup>V. I. Radchenko, Zh. Tekh. Fiz. **62**, 132 (1992) [Sov. Phys. Tech. Phys. **37**, 431 (1992)].

<sup>20</sup>M. S. Dmitriev and V. S. Nikolaev, Zh. Eksp. Teor. Fiz. **44**, 660 (1963) [Sov. Phys. JETP **17**, 447 (1963)].

<sup>21</sup>W. E. Meyerhof, H.-P. Hulskotter, Dai Qiang *et al.*, Phys. Rev. A **43**, 5907 (1991).

<sup>22</sup>L. D. Landau and E. M. Lifshitz, *Quantum Mechanics*, 3rd ed., Pergamon, Oxford (1977).

<sup>23</sup>A. A. Radtsig and B. M. Smirnov, *Handbook of Atomic and Atomic Ion Parameters* [in Russian], Énergoatomizdat, Moscow (1986).

<sup>24</sup>K.-P. Huber and G. Hertzberg, *Constants of Diatomic Molecules* [Russian translation], Mir, Moscow (1984).

Translated by David L. Book